Synthesis of Stoichiometric Cu3BiS3 Thin Films through Sulfurization of Oxide Precursors

Peer-reviewed author version

REIS SANTOS, Daniely; Milano, Lorenzo; JOOS, Bjorn; RUTTENS, Bart; Khurana, Divyansh Anil; D'HAEN, Jan; BOYEN, Hans-Gerd; DESTA, Derese; SHUKLA, Sudhanshu; HARDY, An & VERMANG, Bart (2025) Synthesis of Stoichiometric Cu3BiS3 Thin Films through Sulfurization of Oxide Precursors. In: ACS Applied Energy Materials, 9 (1) , p. 606 -614.

DOI: 10.1021/acsaem.5c03411
Handle: http://hdl.handle.net/1942/48056

Synthesis of stoichiometric Cu_3BiS_3 thin films through sulfurization of oxide precursors

Daniely Reis Santos[1,2,3], Lorenzo Milano[2,3,4], Bjorn Joos[1], Bart Ruttens[1], Jan D'Haen[1], Derese Desta[1], Hans-Gerd Boyen[1], Divyansh Anil Khurana[2,3,5], An Hardy[1,2], Sudhanshu Shukla[1,2,3*], Bart Vermang[1,2,3]*

[1] Hasselt University, Institute for Materials Research, imo-imomec, Martelarenlaan 42, 3500 Hasselt, Belgium

[2] Imec, imo-imomec, Thor Park 8320, 3600 Genk, Belgium

[3] EnergyVille, imo-imomec, Thor Park 8320, 3600 Genk, Belgium Hasselt University, Hasselt, Belgium

[4] Politecnico di Milano, Piazza Leonardo da Vinci 32, 20133 Milan, Italy

[5] cMACS, KU Leuven; Celestijnenlaan 200F, 3001 Leuven, Belgium

Corresponding authors:

daniely.santos@imec.be; sudhanshu.shukla@imec.be

TOC graphic

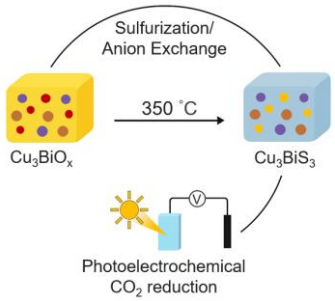
Sulfurization/
Anion Exchange
350 °C
Cu_3BiO_x
Cu_3BiS_3
V
Photoelectrochemical
CO_2 reduction

Abstract: The wittichenite-type compound (Cu_3BiS_3, CBS) shows great potential for photovoltaics and solar-to-fuels applications due to its favorable optoelectronic properties. However, precise control over composition and phase stability in thin films remains challenging to achieve due to phase complexity and a limited kinetic stability window. This research focuses on obtaining homogeneous and stable CBS phases with ideal composition through a simple sulfurization process of an oxide Cu-Bi-O (CBO) precursor film in the thermodynamically permissible temperature range (350 - 425 $^{\circ}$C). The findings confirm successful conversion of oxide film to wittichenite phase, free of secondary phases, at 350 $^{\circ}$C with a direct bandgap energy of 1.61 eV. The energy band positions from photoelectron spectroscopy show favorable energetics towards water splitting and CO_2 reduction. Photoelectrochemical performance of a prototype CBS/TiO_2 heterojunction device demonstrates photocurrent density of 0.12 mA/cm^2 and 0.96 mA/cm^2 for water splitting and CO_2 reduction, respectively. The presented method can be further explored to fabricate CBS films in various configurations for PEC and solar cell devices.

Keywords: Cu_3BiS_3; wittichenite; sulfurization; solar energy conversion; photo electrocatalysis;

1. Introduction

Bismuth-based chalcogenide (BC) compounds have drawn considerable attention for several energy harvesting systems, such as photothermal,[1] photo(electro)catalytic,[2] and photovoltaic applications.[3] Recently, the orthorhombic and ternary copper-bismuth chalcogenide I–V–VI compound, Cu_3BiS_3 (CBS), has spurred interesting characteristics owing to its favorable optoelectronic properties such as an outstanding high optical absorption coefficient ($\alpha > 10^5$ cm^{-1}) in the visible region, a pseudo-direct band gap ($E_g \approx 1.10–1.86$ eV),[4] and its apparent p-type conductivity.[5] Additionally, it is stable at room temperature[6] and found in nature as the wittichenite mineral.[7] These properties make CBS a promising candidate for a low-cost energy harvesting system,[8] particularly photovoltaics and photoelectrochemical cells.

A key challenge in the synthesis of pure-phase CBS is the lack of an adequate understanding of its phase diagram, which is essential for guiding the synthesis and ensuring the formation of a pure phase with minimum defects. The CBS phase diagram shows that the compound Cu_3BiS_3 is formed in a narrow compositional range, with a stability domain from 350 to 527 $^{\circ}C$,[9] which highlights the challenges in obtaining a pure phase with the desired stoichiometry (i.e., 3:1:3). Moreover, the phase diagram also highlights the importance of precisely controlling the temperature during the synthesis process since minor deviations can lead to the formation of secondary phases (such as Cu_2S or Bi_2S_3) or variation in the stoichiometric composition (e.g., $CuBiS_2$, $Cu_4Bi_4S_9$). Several reports on vacuum and non-vacuum-based synthesis techniques include co-evaporation, sputter deposition, spray pyrolysis, chemical bath deposition, and electrodeposition.[4] Despite several efforts, producing high-quality CBS thin films without any phase impurities remained challenging. This is exemplified in terms of the low power conversion efficiency of 1.7 % for the best CBS solar cell reported so far.[10] Hence, an adequate understanding of its fabrication and complete

characterization is necessary before testing the material for different applications. There are many critical challenges for the integration of CBS into efficient systems, mainly two fundamental aspects: i. the establishment of reproducible growth of a pure phase material, and ii. a comprehensive understanding of its optoelectronic properties. Therefore, maintaining the correct temperature and stoichiometry during the synthesis is essential to balance both kinetic and thermodynamic factors, ensuring the process remains within the stability domain. Beyond the challenges of obtaining a suitable stoichiometry, there has been limited study of their photoelectrochemical applications. While CBS has been previously explored for photoelectrochemical water splitting[11], its potential for CO_2 reduction has not been thoroughly investigated.

In this study, we investigated the conversion of oxide to sulfide *via* anion exchange, focusing on understanding the sensitivity towards secondary phase formations throughout the process. We evaluate the influence of processing temperature on the formation of different phases and understand the phase transformation mechanism to identify the ideal conditions for forming Cu_3BiS_3 pure phase. Here, we synthesized CBS using a two-step approach. First, copper-bismuth-oxides (CBO) thin films were prepared with a proper stoichiometric composition (Cu/Bi, 3:1) using an aqueous chemical solution deposition (CSD) route *via* spin coating[12] and converted to CBS by the sulfurization process *via* a solid-gas reaction. The oxide-based conversion approach offers a promising strategy for effective synthesis, aiming at controlling the formation of specific phases.[13] This is because oxides are chemically more stable than sulfides,[14, 15] exhibit greater thermal stability, and are easier to control during deposition processes. Moreover, a controlled sulfurization process allows the navigation of complex phase space, which reduces the probability of formation of secondary phase(s). Beyond the synthesis of CBS, this study conducts a

comprehensive investigation of topography, optical properties, oxidation states, and energy band positions within the temperature range of 350 – 425 °C (i.e. within the stability window). PEC water splitting measurements are presented as a benchmark to confirm the photoactivity of the films. Additionally, we evaluated the PEC CO_2 reduction activity of CBS in a CO_2-saturated electrolyte, providing initial insights into its suitability as a CO_2R photocathode.

2. Experimental section

2.1 Fabrication of Cu_3BiS_3 thin film

CBS films were obtained by a two-stage process: (i). copper-bismuth-oxide (CBO) precursor obtained by solution processing using aqueous CSD and (ii). sulfurization of CBO to obtain copper-bismuth-sulfide (CBS), as schematically shown in Figure 1.

The synthesis procedure of copper-bismuth oxide has been described elsewhere by Joos *et al*.[12] Briefly, the fluoride-doped Tin oxide (FTO) deposited on soda lime glass (SLG) (FTO/SLG) was used as a substrate (Sigma Aldrich). Prior to the processing, the substrates were cleaned sequentially in deionized water and acetone, followed by 30 min of UV-Ozone treatment to improve the surface's wettability. The multi-metal ion solution was obtained by mixing a copper-based solution containing copper(II) formate tetrahydrate and a bismuth-based solution containing bismuth(III) citrate (3:1 stoichiometric molar ratio). The final multimetal ion precursor was deposited *via* spin-coating at 3000 rpm for 30 seconds. The films were deposited by five consecutive spin-coating cycles, each followed by drying/heating steps at 120 °C, 270 °C, and 480 °C to remove organics and convert the precursor to oxide. This resulted in a total film thickness of ~350 nm. The films were then annealed at 480 °C for 2 h to achieve full crystallization in the CBO layer.

The second stage involved sulfurising the 3:1 CBO oxide thin film using a two-zone tube furnace. The tube furnace is equipped with two thermocouples, one located on the left side and the other on the right side. These thermocouples continuously measure the temperature at their respective positions, providing real-time feedback to the furnace's control system. During the process, a crucible containing 0.5 g of sulfur (S) powder and precursor CBO film was placed in different heating zones of the tube furnace at 200 $^{\circ}$C and (350 - 425 $^{\circ}$C), respectively (Fig. 1). Subsequently, the tube was purged with N_2 gas three times and then filled with N_2 to create an inert atmosphere. In the annealing step, the thin film precursor was heated to the desired temperature (T_x = 350, 375, 400, or 425 $^{\circ}$C) for 20 minutes, held for 30 minutes, and then allowed to cool naturally. In contrast, during the sulfur thermal cycle, the temperature was set at 200 $^{\circ}$C for 45 minutes, with a ramping rate of 13.3 $^{\circ}$C min^{-1}. The ramp-up in sulfur is shorter compared to the sample's annealing process to ensure a S-rich atmosphere. The annealing profile is shown in Figure S1.

2.2 Characterization of thin-film photo absorber

CBS thin films' morphological characteristics and cross-section were obtained by high-resolution scanning electron microscopy (SEM) analysis (TESCAN Vega3 SBU) operated at 15 kV. The energy-dispersive X-ray spectrometer (EDX) (Bruker XFlash 610M) operated at 15 kV was employed to evaluate the elemental composition of the copper-based oxide thin film subjected to sulfurization. The resulting elemental compositions are semi-quantitative and were used to compare relative changes in elemental concentrations across samples rather than to determine absolute compositions. The crystallinity and phase formation were determined by X-ray diffractometry (XRD) using a Bruker D8 equipped with a Cu-Kα (λ = 1.5418 Å) radiation source operating at 40 kV and a LYNXEYE detector. Complementary to XRD, Raman spectroscopy,

Renishaw VirsaTM analyzer, was employed to confirm the phases formed in the sample. A laser excitation of 532 nm with a power of 10 mW, a spot size of 1 μm, and an Olympus 100X long working distance objective was used for the measurements. To estimate the bandgap of the CBS thin film, samples were tested by visible and near-infrared (NIR) spectroscopy (Bentham 605). Optical reflectance and transmittance were recorded using a 3.7x3.7 mm^2 filter and both Si and Ge detectors (covering a total range of 400 - 1400 nm wavelength). The optical absorption (A) and the absorption coefficient (α) were calculated according to equations 1 and 2, respectively. To estimate the bandgap, the Tauc Plot method (Eq. 3) was employed, in which n corresponds to the transition type (direct or indirect allowed/forbidden transitions) and E_g corresponds to the bandgap value for CBS. The core-level and valence band (VB) spectra of the CBS sample were acquired using X-ray photoelectron spectroscopy (XPS) and ultraviolet photoelectron spectroscopy (UPS). Both measurements were conducted in an ultrahigh vacuum chamber with a base pressure of 10^{-9} mbar. For the XPS experiments, a monochromatized Al Kα radiation source (hν= 1486.6 eV) operated at 300 W was used as the excitation source, achieving an overall energy resolution of 0.36 eV full width at half maximum (FWHM). The UPS measurements employed a He I gas discharge lamp (hν= 21.2 eV), which provided significantly improved energy resolution.

$$A = \frac{T}{(1-R)} \times 100\% \quad \text{(Eq. 1)}$$

$$\alpha = \frac{2.303 \times A}{d} \quad \text{(Eq. 2)}$$

$$(\alpha h\nu)^{\frac{1}{n}} = A(h\nu - E_g) \quad \text{(Eq. 3)}$$

2.3 Photoelectrochemical studies

TiO_2 blanket layers were deposited on CBS *via* atomic layer deposition to create a p-n heterojunction using ALD R200 from Picosun. Titanium tetrachloride ($TiCl_4$) was used as the Ti

precursor, and H_2O was the oxidizing agent. The reactor chamber was maintained at 250 °C, and the substrate was subjected to 1000 cycles of each of the Ti and oxidizing precursors to deposit a 50 nm layer.

Photoelectrochemical measurements were performed using a 3-electrode system containing a working electrode (CBS/TiO_2), a counter electrode (carbon electrode), and a reference electrode (Ag/AgCl, 3M KCl). In order to identify the performance of the material, linear sweep voltammetry was conducted. For that, 0.1 M Na_2SO_4 (pH 7.4) or 0.1 M $KHCO_3$ (pH 8.0) were used as a supporting electrolyte. All the experiments were performed using an Oriel light source equipped with a 150 W Xe lamp (100 mW cm^{-2}) for illumination. The potential values were converted with respect to RHE using Equation 4.

$$E_{RHE} = E_{Ag/AgCl} + 0.059pH + 0.197 \quad \text{(Eq. 4)}$$

3. Results and discussion

The synthesis of polycrystalline copper bismuth sulfide thin films was performed by thermal sulfurization of copper-bismuth-oxide (CBO) precursor thin films, as described in section 2. Figure 1 represents the basic scheme of the oxide-to-sulfide conversion process. We investigated the phase distribution and optoelectronic properties of the CBS films obtained after sulfurization of oxide films within a temperature range of 350 - 425 °C. The conversion of the oxide film is suggested to proceed through a gas-phase anion exchange reaction, where anions such as S^{2-} from the gas phase react with the precursor. The final structure of the film is governed by the annealing temperature. The Cu:Bi stoichiometric ratio was maintained at 3:1 in the precursor films to achieve the final stoichiometric Cu:Bi ratio of 3:1 in the aimed Cu_3BiS_3 thin films. The composition ratio of each element in CBO was analyzed through EDX (Supplementary Table 1, showing that the

atomic ratio of the oxide precursor was very close to the expected ratio). The SEM image showed a compact and uniform continuous morphology for the CBO samples, with small grain sizes (Figure S2).

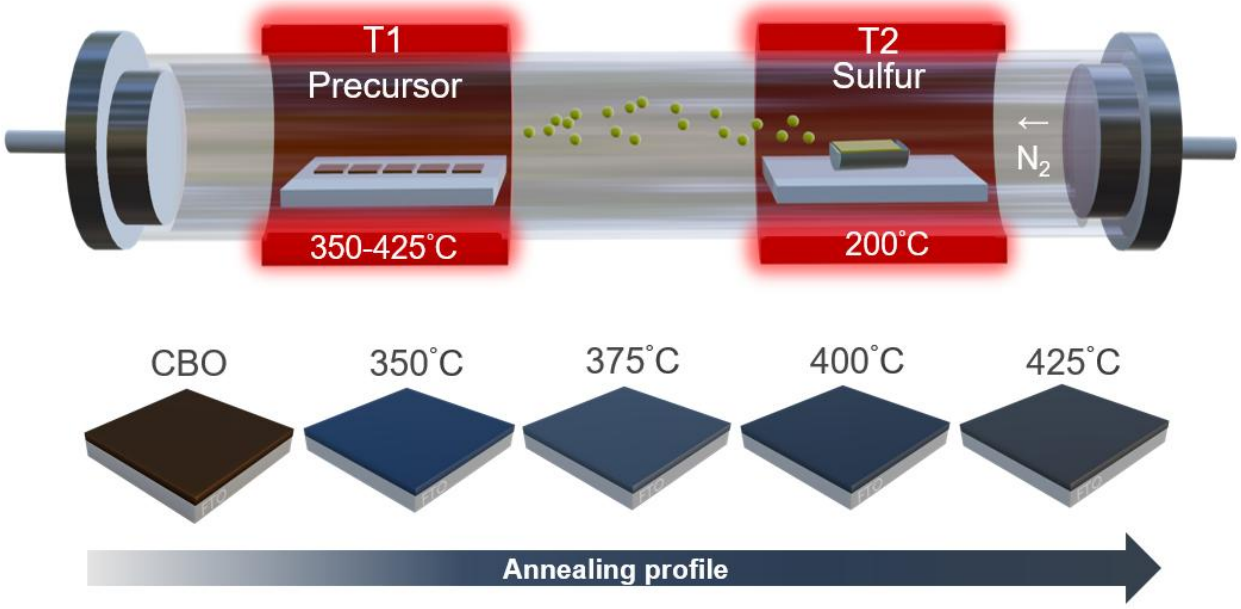

Figure 1 Schematic illustration of the fabrication of copper-bismuth-sulfide (CBS) *via* sulfurization of a copper-bismuth-oxide (CBO) precursor on FTO substrates. Two heating zones (T1-thermal couple 1 and T2-thermal couple 2) are presented for precursor and sulfur annealing.

Effect of annealing temperature on crystallinity and phase distribution. XRD analysis was performed to identify the crystal structure and phases formed after the sulfurization process at 350, 375, 400, and 425 ˚C, and are shown in Figure 2. The dominant peaks at 26.4 ˚, 33.7 ˚, 37.7 ˚, and 51.5 ˚ are ascribed to the FTO (F:SnO_2) substrate. The wittichenite pure phase was obtained for all temperatures with diffractogram peaks well indexed with the wittichenite orthorhombic structure, space group 19, $P2_12_12_1$, JCPDS No. 01-071-2115.[7] This is better observed in the specific two theta ranges (10 ˚ - 24 ˚) and (27 ˚ - 33 ˚), as shown in Figures 2b and c. We also note that impurities

or other secondary/ternary phases related to Cu_2S and Bi_2S_3 ($6CuS + Bi_2S_3 \rightarrow 2Cu_3BiS_3 + 3S$)[16] or $Cu_4Bi_4S_9$ ($8CuS + 4Bi_2S_3 \rightarrow 2Cu_4Bi_4S_9 + 2S$)[17] were not observed (Figure S3), indicating that the conversion process bypasses these secondary phases.

Although the CBS phase appeared at 350 °C, the sulfurization temperature has a strong influence on the crystalline quality of the film. Therefore, we increased the sulfurization temperature in steps (375, 400, and 425 °C) to explore the temperature window that promotes the formation of wittichenite phase and enhances crystallinity. As the temperature increases, XRD peaks became narrower and more intense, consistent with grain growth and reduced structural disorder due to enhanced atomic diffusion and recrystallization[18]. Similar temperature-dependent improvements in crystallinity have been reported for other copper-chalcogenide thin films, attributed to thermally activated grain coalescence and defect annealing[19]. However, at temperatures above 350 °C, secondary phases start to appear (see Fig. S4), likely due to sulfur loss and cation interdiffusion that disturb the stoichiometry of the CBS phase. This behavior suggests that CBS phase stability is governed by a delicate balance between thermodynamic driving forces for crystallization and kinetic limitations related to sulfur volatility and element diffusion at elevated temperatures.

Raman spectroscopy was also performed in order to confirm the formation of the phases, as shown in Figure 2d. For all the temperatures studied, Raman spectra showed two main peaks at 279.3 and 471.0 cm^{-1}. These were attributed to the pure Cu_3BiS_3 phase, matching well with spectra previously reported for the wittichenite phase.[20] The peak centred at 279 cm^{-1} is observed to contain an additional shoulder at lower frequencies for all sulfurization temperatures. Upon deconvolution, the 350 °C annealed film renders this additional shoulder peak at around 263 cm^{-1} (Figure S5). This peak is attributed to the other CBS Raman-active mode at around 263 cm^{-1}, as reported by Whittles *et al.*[21] It is not clear why it appears only at low annealing temperatures. A possible

explanation could be the presence of an amorphous CBS phase that is Raman active, as corroborated by a broad signature of the peak.

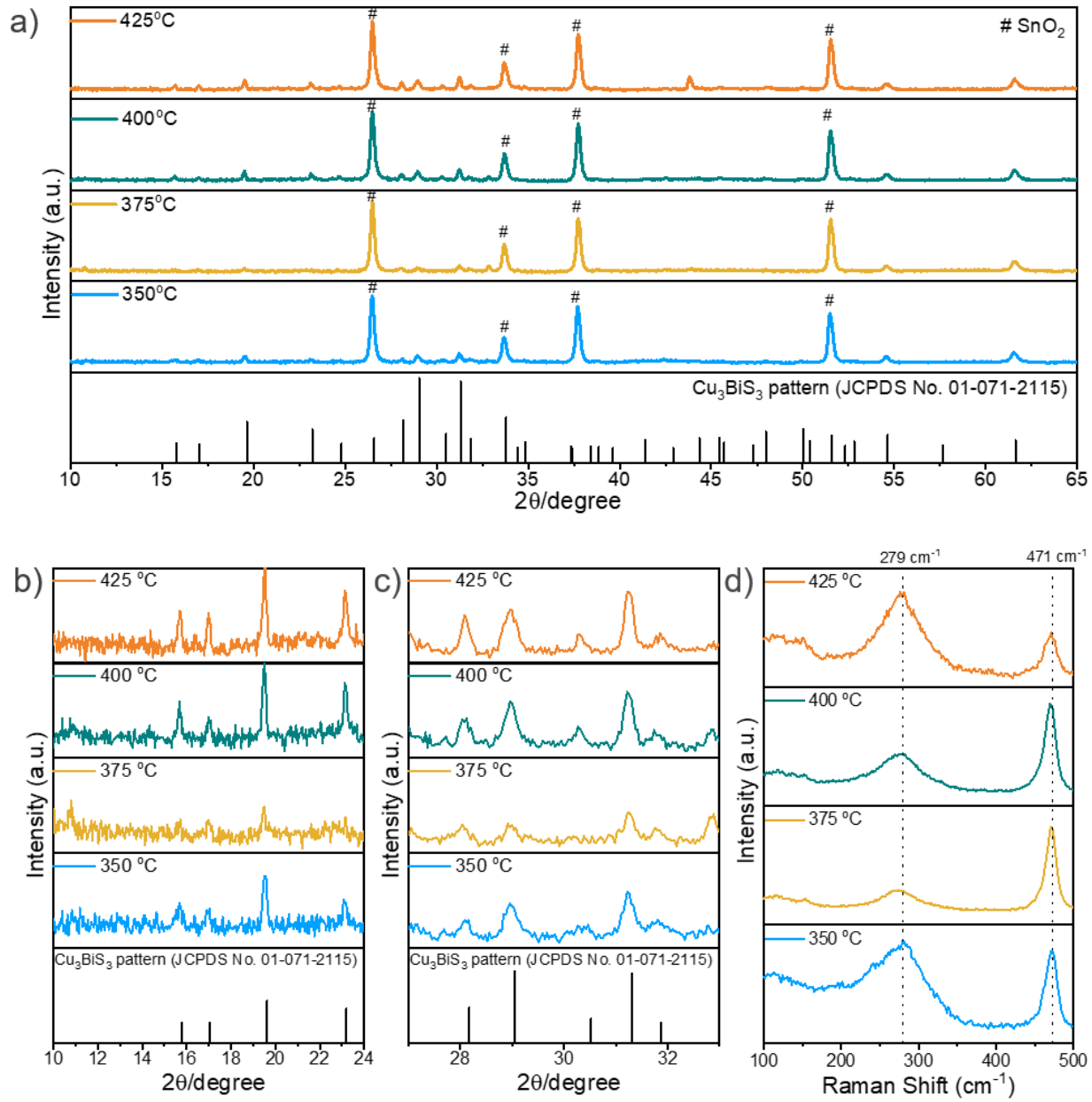

Figure 2 XRD diffractogram **a.** full scan, and magnified scan in the two-theta range, **b.** 10 – 24 °, and **c.** 27 – 33 °; **d.** Raman spectra of the CBS films obtained after the sulfurization of CBO precursor films at different temperatures (350 – 425 °C).

Effect of temperature on grain formation and composition. One of the critical features of thin films is characterized by grain growth, and temperature plays a crucial role in determining it. The surface morphology of the CBO thin film sulfurized at different temperatures is shown in Figure 3. Through SEM images, it is possible to observe a significant surface morphological change of CBS thin films annealed at different temperatures. A compact film with particles on its surface is observed at low temperatures. Besides, it is noticed that the morphology of the phase-pure CBS is free of pinholes and other imperfections. An increase in temperature leads to the coalescence of grains through diffusion-enhanced grain growth, facilitating the migration and merging of grain boundaries.[22] This is clearly observed, especially above 400 °C. EDX results reveal that increasing the sulfurization temperature promotes sulfur ingress in the film, as shown in Figure 3b and Table S2. Cross-sectional SEM images (Figure S6) reveal that the CBO precursor and the film sulfurized at 350 °C (Figure 6b) maintain its initial thickness (~350 nm). This can be attributed to the correct stoichiometry of the precursor, confirming that the sulfurization involves mainly substitution of O by S, rather than large-scale cation diffusion or loss to correct the composition. With an increase in temperature, morphological changes are noticed during the sulfurization process. At 375 °C, slight densification and a reduction in thickness (~300 nm) are observed, and EDX analysis reveals Bi enrichment, Cu depletion, and an increase in sulfur content, suggesting partial sulfide formation (Table S2). Upon further heating to 400-425 °C, the Bi content gradually decreases, while Cu continues to decline, and sulfur incorporation reaches its maximum. The reported EDX trends are qualitative, intended to compare relative elemental changes rather than provide absolute composition. The film exhibits pronounced grain coalescence and surface roughening, with an apparent thickness increasing up to ~400 nm. These results reflect the interplay between densification, diffusion-enhanced grain growth, cation redistribution, and sulfur incorporation.

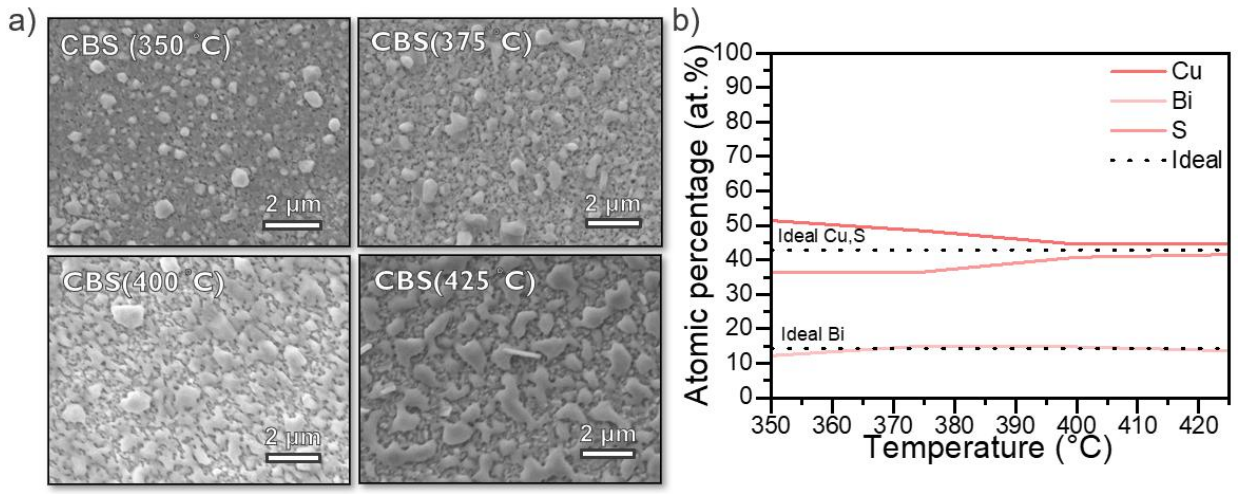

Figure 3. a. SEM image showing the morphological evolution with increasing temperature; **b.** EDX spectra of the sulfurized samples confirm the elemental composition and presence of Cu, Bi, and S in CBO precursors sulfurized at different temperatures (350 – 425 °C). The reported atomic percentages (at.%) are included to indicate the approximate elemental proportions.

Optoelectronic properties. The bandgap of the CBS films formed from CBO precursors was determined using UV-Vis measurements. Copper-based oxide materials have a higher bandgap compared to copper-based chalcogenide materials. This is reportedly because chalcogen atoms have a lower electronegativity compared to oxygen, leading to weaker bonding,[23] and due to a difference in its defect chemistry. [14] This was shown by comparing the transmission for the CBO precursor film and the final CBS film. A decrease in transmission at wavelengths between 400 and 1200 nm in the CBS film compared to the CBO precursor implies a reduction in the bandgap after the sulfurization of CBO (Figure S7).

UV/Vis absorption spectra of the CBS thin films reveal distinct features corresponding to their electronic transitions (Figure S7b). At higher photon energies (> 2.0 eV), the sample annealed at 350 °C exhibits the highest absorption, suggesting improved film uniformity and optical quality.

More interestingly, at around 0.8–1.2 eV, which is expected to lie within the electronic bandgap of the CBS films, a lower energy tail is observed, and may be attributed to sub-bandgap states and defect-related absorption[24]. Furthermore, the absorption coefficient (α) was calculated from the measured absorption profile via the Tauc plot method, which enabled the estimation of the optical band gap. The linear dependence of $(\alpha h\nu)^2$ on hν (Fig. 4a) suggests that the electronic transition in CBS corresponds to a direct allowed transition. The absorption coefficient of the resulting Cu_3BiS_3 from CBO sulfurization at 350 °C showed a high $\alpha \sim 10^6$ cm^{-1} (at 1.61 eV, Fig. S8). The bandgap values of 1.61, 1.57, 1.38, and 1.38 eV (individual linear fits shown in Figure S9) were estimated for CBS films obtained after sulfurization at 350, 375, 400, and 425 °C, respectively, lower than the corresponding oxide ($CuBi_2O_4$) bandgap[12] and consistent with the range of values (1.0 – 1.81 eV) reported in the literature.[4] The direct optical transition behavior, along with considerable band-tailing in the spectra, indicates the high defect concentration in the CBS film.[23] The bandgap successively reduces as the sulfurization temperature increases, most likely due to the contribution of secondary phases, whose existence was inferred from the XRD patterns discussed previously (see Fig. S4). A correlation is found between the change in the bandgap and the composition. Figure 4b shows that the Cu/Bi ratio and bandgap concomitantly decrease with sulfurization temperature.

For relevance of a semiconductor electrode in photoelectrochemical applications, its band edges must be suitably positioned in reference to the redox potentials for the reactions of interest. This is because the necessary driving force for the photogenerated carriers to contribute to redox reactions is provided by the energetic (mis)alignment of the energy bands with the electrochemical potential of the redox species in the electrolyte. For instance, for photoelectrochemical water splitting, the conduction band minimum (CBM) should be higher in energy than the potential for

hydrogen evolution reaction (HER) to allow for reduction of water by photo-electron capture at CBM. Similarly, the valence band maximum (VBM) should be lower in energy than the potential for oxygen evolution reaction (OER) to allow for water oxidation from capture of the photogenerated holes at the VBM.[25] Owing to the potential of HER being 0 V vs RHE and potential for OER being 1.23 V vs RHE, the bandgap of the semiconductor must be greater than 1.23 eV. Furthermore, since the electron-transfer processes at the semiconductor/liquid junctions produce losses (i.e. from electrolyte and circuit resistances, kinetic overpotentials, etc.)[26], additional energy inputs are necessary to account for the losses. Therefore, in principle, an energy input higher than 1.5 eV is required (illustration shown in Figure S10). Considering that the CBO precursor sulfurized at 350 °C showed a pure wittichenite phase and a suitably high bandgap (1.61 eV), a detailed study was conducted to infer its band-edge positions.

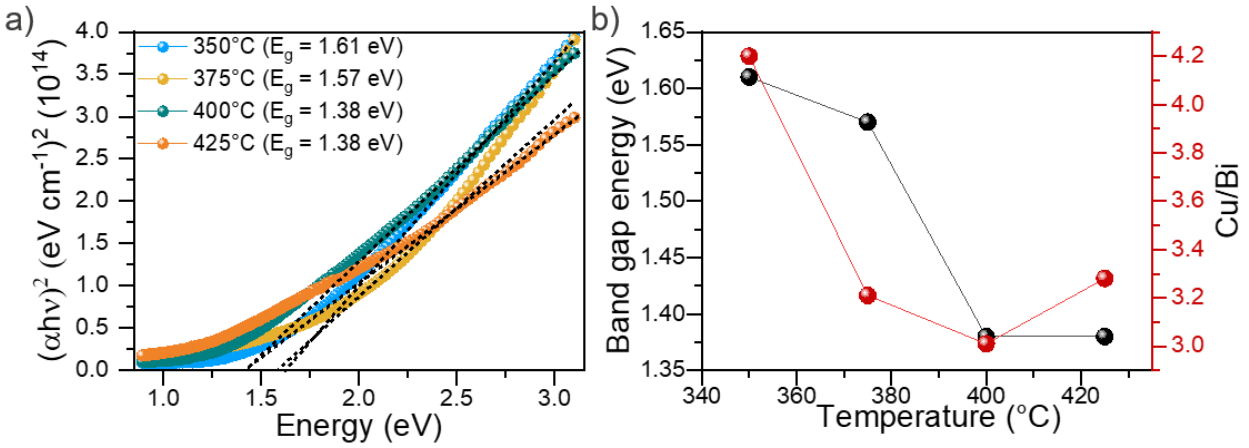

Figure 4. a. Tauc plot and **b.** correlation of bandgap, temperature, and Cu/Bi elemental ratio for CBO precursor sulfurized at different temperatures (350 – 425 °C).

Oxidation states and characterization of energy band positions. X-ray photoelectron spectroscopy (XPS) was performed on the CBS films to determine the oxidation state of the film constituents (see Fig. 5). With only few XPS studies on CBS thin films in the literature, we

emphasized the need of careful fitting of the overlapping Bi 4f and S 2p peak. A fitting procedure from Whittles *et al.*[21] was used to analyze the peaks in this work accurately. Peaks from Cu, Bi, and S were observed in the XPS survey scans of the surface of all the CBS films, in addition to signals from C and O contaminants (Figure S11a). Cu 2p, Bi 4f, and S 2p spectra are shown in Figure 5. Cu 2p showed a doublet (with a peak splitting of 19.8 eV) that was assigned to Cu^{1+}. The absence of a satellite peak from Cu^{2+} at 942 eV suggests that impurities, such as CuS, did not form, corroborating the XRD and Raman results. The Bi 4f and S 2p core level regions for CBS are also shown in Figure 5b. The spectra reveal two bismuth components at 163.3 and 158.0 eV (with a splitting of 5.3 eV), which are attributed to CBS and assigned to Bi^{3+}. Another doublet at 163.9 and 158.7 eV is associated with bismuth oxide (Bi_2O_3), likely formed as a result of surface exposure to the air. This difference in XPS and XRD analysis can be explained by their respective probing depth, with the former providing more surface-sensitive (~ 5-10 nm) and the latter containing more bulk information. Finally, a third doublet, represented in yellow, is assigned to S^{2-} and corresponds to S 2p. Additionally, a singlet is observed at around 225 eV (Fig. S11b), attributed to the S 2s region. This singlet is remarkable and not commonly reported.

Ultraviolet photoelectron spectroscopy (UPS) was performed on the CBS electrode to determine the valence band maximum (VBM). The intercept was determined with the Multipak software's Edge tool using a linear approximation[27]. Figure 5c shows the unbiased UPS for CBS at room temperature. VBM for CBS was found to be 0.13 eV with respect to the Fermi level (i.e., E_F-E_{VB} = 0.13 eV). Further, considering the relation of CBM = VBM + E_g, it is possible to determine the energetic position of the CBM. Based on these derivations, we attempt to draw the full energy band diagram of the CBS and its correspondence with typical redox reactions. Figure 5d shows the band-edge position for CBS, where the energy values are referenced to the normal hydrogen

electrode (NHE). CBS exhibited p-type behavior, as the Fermi level was located very close to the VBM, as determined from the UPS measurements. The VBM, however, existed at energies higher than the potential for OER, which does not allow for an isoenergetic hole capture by the reductant density of states in water at VBM, making CBS inefficient for OER. Nonetheless, it is inferred that the CBM was appropriately positioned at higher energies (CBM >> potential for HER), so that HER was enabled from the isoenergetic capture of photo-electrons at the CBM. In fact, the highly negative CBM and a small enough bandgap to allow absorption of the visible spectrum make the p-type CBS electrode an interesting candidate for photo-electrochemical CO_2 conversion applications (see Fig. 5d).

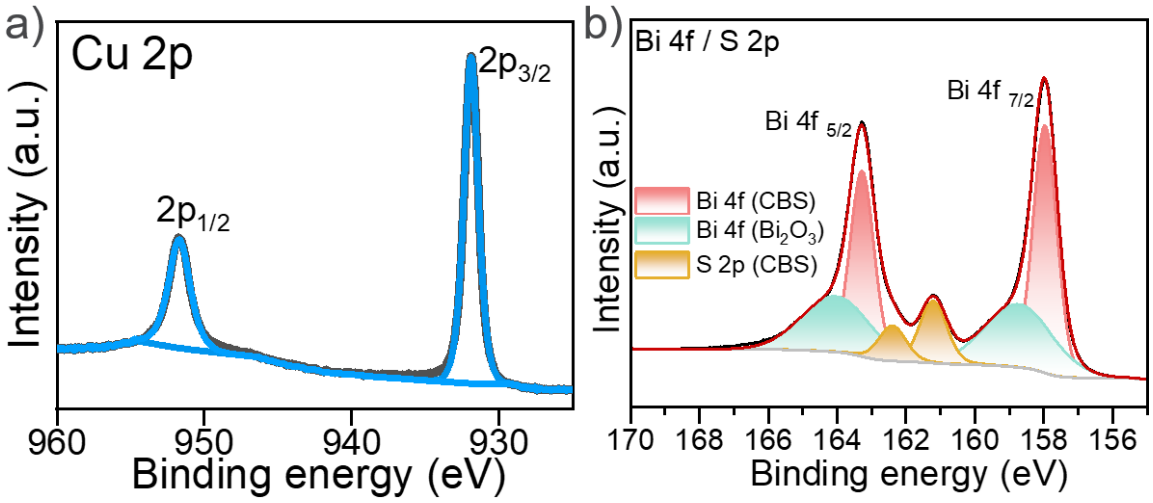

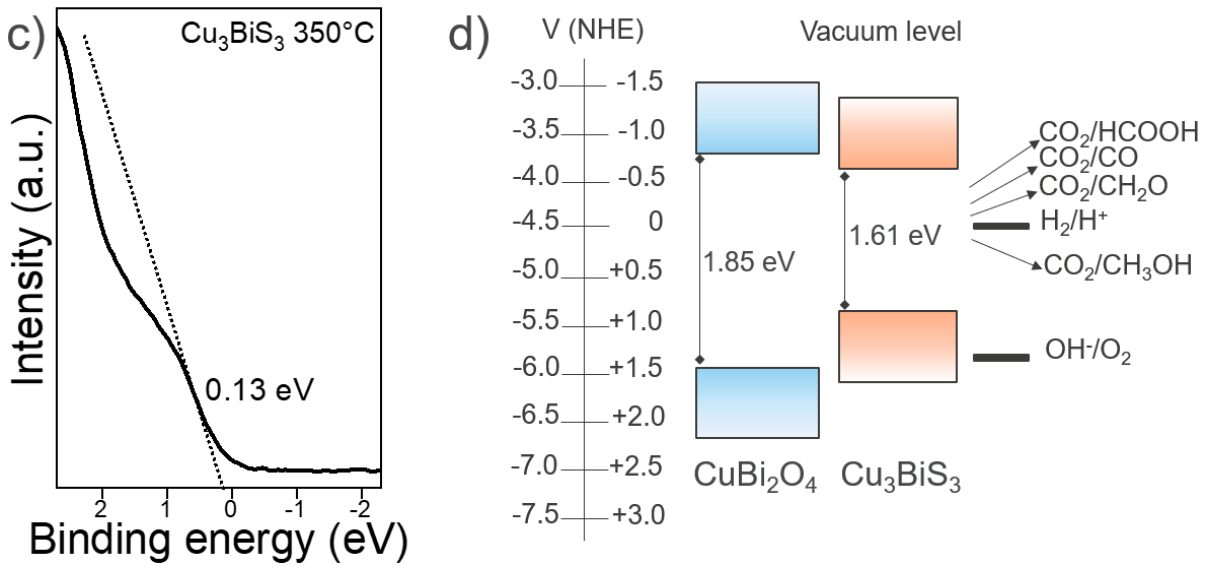

Figure 5 a. XPS spectra for the Cu 2p region and **b.** Bi 4f and S 2p overlap region of the CBO sulfurized at 350 °C; **c.** Unbiased VBM UPS spectra with linear fits and **d.** a comparison band alignment for the most known copper-bismuth-oxide, $CuBi_2O_4$, and CBS with respect to the H_2 production and CO_2 reduction potentials reactions.

p-n heterojunction for photoelectrochemical tests. To investigate the performance of CBS for cathodic applications (reduction reactions), a photoelectrochemical (PEC) setup was employed, as shown in Figure 6a. A 3-electrode PEC cell was formed, where the CBS-based photocathode, a carbon electrode, and a 3M KCl Ag/AgCl electrode served as the working, counter, and reference electrodes, respectively. The current-potential (i-U) characteristics were obtained both in darkness and under a constant 1 sun illumination. We evaluated the photoelectrochemical behavior of CBS in 0.1 M Na_2SO_4, saturated with N_2 (pH 7.4) (Figure 6a), and 0.1 M $KHCO_3$, saturated with CO_2 (Figure 6b), as these electrolytes are the most commonly used in PEC applications.[28] While Na_2SO_4 provided a neutral, inert, and stable environment for hydrogen production without interference from side reactions, $KHCO_3$ created a buffered system with the dissolved CO_2

supplied for efficient photoelectrochemical CO_2 reduction. A 50 nm thin-film of n-type TiO_2 was deposited by atomic layer deposition (ALD) on the ~300 nm thin film of p-type CBS to construct a p-n heterojunction. The built-in electric field at the heterojunction, in addition to an external bias, would enable the separation of photo-generated charge carriers and suppress recombination. The TiO_2 film may further passivate the defect states at the CBS surface, and also protect it from parasitic reactions with the electrolyte. It should also be noted that owing to the typical large bandgap of TiO_2 (> 3.0 eV), it is expected to be transparent to the visible spectrum incident on the electrode, and any photo-absorption therefore must occur in the CBS film. Figure 6 shows the current-potential (i-U) characteristics from a linear sweep voltammogram (LSV) for the CBS/TiO_2 photocathode under darkness and in light, in both electrolytes. For CBS in N_2-saturated Na_2SO_4 electrolyte in darkness, the currents remained near 0 mA cm^{-2}. However, when illuminated, a non-zero current was measured at the electrode-electrolyte interface. Although small, still -0.12 mA cm^{-2} of photocurrents were achieved at -0.2 V vs. RHE. In case of the CO_2-saturated $KHCO_3$ electrolyte in darkness and scanning negative potential, the current remained stable at 0 mA cm^{-2} down to 0.1 V vs. RHE, below which the dark currents increased slightly, reaching -0.25 mA cm^{-2} at -0.1 V vs. RHE. When illuminated, the photocurrents increased significantly and reached -0.95 mA cm^{-2} at -0.1 V vs. RHE, representing a nearly fourfold increase from the dark current. In fact, the cathodic photocurrents in illuminated CO_2-saturated electrolyte were 8-fold compared to the N_2-saturated electrolytes, at 0 V vs RHE. Additionally, a cathodic shoulder was observed at around 0.5 V vs RHE in the CO_2-saturated but not in the N_2-saturated electrolyte and may therefore be ascribed to bicarbonate ions (HCO_3^-) or adsorbed CO_2 intermediates. A CBS/TiO_2 heterojunction electrode was further subjected to a constant potential of 0 V vs RHE in the CO_2-saturated electrolyte to evaluate its stability and (photo-)electrochemical CO_2 reduction performance under

continuous illumination. The associated current transients are given in Figure 6d. The photocurrent initiated from a large negative value at t = 0 s (-0.4 mA cm^{-2}) and then plateaued at –0.1 mA cm^{-2} at t > 200 s without any significant decay, going up to 1200 s (= 20 mins) of operation. The observed photocurrent during the first few seconds arises from non-Faradaic processes, including double-layer charging and surface-state filling[29]. After this, the photocurrent stabilizes at −0.10 mA cm^{-2}, which represents the true steady-state faradaic response of the photoelectrode. This indicated that the CBS/TiO_2 heterojunction possessed good operational durability for (photo)electrochemical CO_2 reduction. These results suggest that the CBS/TiO_2 may interact favorably with CO_2 under illumination. In other words, the presence of CO_2 could facilitate interfacial reactions at the photocathode surface, indicating that the CBS/TiO_2 has potential for CO_2 reduction applications. However, since the electrolyte composition also changed between the N_2-saturated and CO_2-saturated electrolytes, the possibility of enhanced water oxidation or alternative parasitic reaction pathways, instead of CO_2 reduction, cannot yet be fully ruled out. Future work will include systematic control experiments with CO_2-free $KHCO_3$ electrolyte and direct detection of CO_2 reduction products to confirm CO_2 reduction activity. To contextualize the performance of CBS in PEC CO_2R, a comparison with literature reports is provided in Table S4. Although the activity and stability are moderate compared to CBS applied to hydrogen evolution reaction (HER) and water splitting applications, this work represents the first use of CBS in CO_2R. Moreover, exploring alternative n-type buffer layers, such as In_2S_3,[30] could improve the charge transfer. Additionally, a co-catalyst (e.g., Au or Ag) on the surface may be explored to improve the reaction kinetics further.[31]

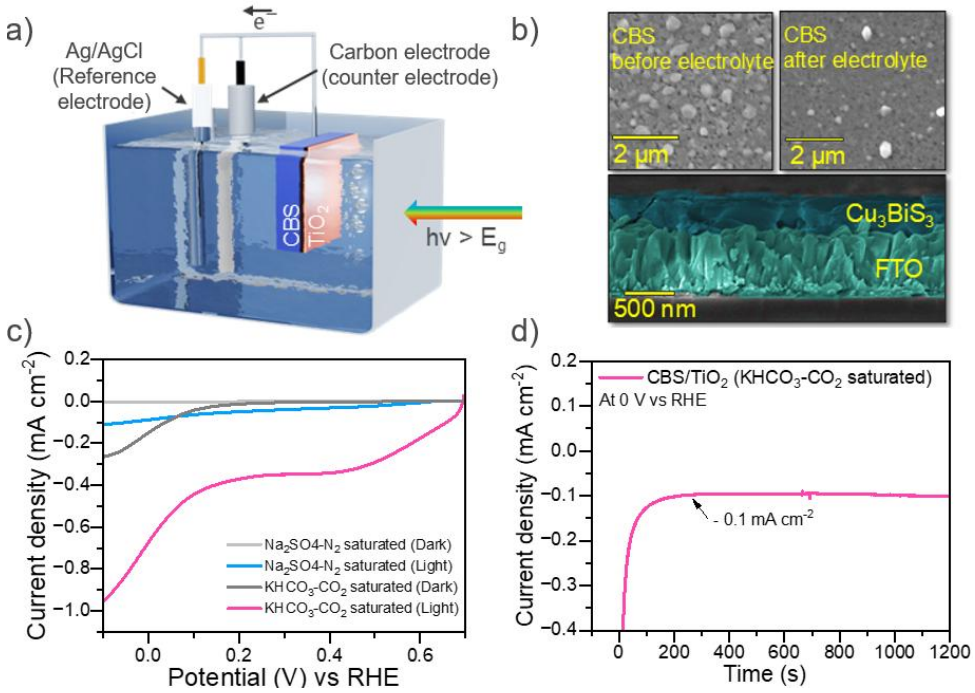

Figure 6 a. Schematic illustration of the PEC setup; **b.** Top surface SEM image before and after CBS immersion in the electrolyte and cross-section SEM of FTO/CBS; **c.** Linear Sweep Voltammetry (LSV) for copper-bismuth-oxide precursor sulfurized at 350 °C in different supportive electrolytes: 0.1 M Na_2SO_4 (pH 7.4) saturated with N_2 and 0.1 M $KHCO_3$ (pH 8.5) saturated with CO_2; **d.** Current transients up to 1200 s for CBS in CO_2-saturated $KHCO_3$ electrolyte at a constant applied potential bias of 0 V vs RHE.

4. Conclusions

The Wittichenite Cu_3BiS_3 phase was successfully obtained by sulfurizing the CBO precursor at 350 °C with a bandgap of 1.61 eV, and the bandgap successively reduced as the sulfurization temperatures increased. UPS results showed that the band edge positions are suitable for (photo)electrochemical HER and CO_2 reduction reactions. The photoelectrochemical performance of a CBS/TiO_2 heterojunction in 0.1 M Na_2SO_4 electrolyte was evaluated. We found that the TiO_2 heterojunction effectively separated the photogenerated carriers in CBS, and the corresponding

PEC device delivered a photocurrent density of 0.12 mA/cm^2. However, in CO_2-saturated $KHCO_3$ aqueous electrolyte, photocurrent density was slightly enhanced (-0.95 mA cm^{-2} at -0.1 V *vs* RHE), suggesting that the CBS/TiO_2 heterojunction was viable for CO_2R. Further studies are required to suppress bulk recombination and enhance carrier separation using electron transport and hole transport layers, ETL and HTL, respectively, thereby improving photocurrent density and increasing selectivity towards PEC hydrogen or CO_2 reduction. Further exploration of co-catalysts to facilitate electron transfer is also highly recommended.

Supporting Information

Annealing profile, SEM images, EDX analysis, XRD diffractograms, Raman spectra, cross-section SEM, UV-Vis spectra, single-fitting Tauc plots, XPS survey, XPS peaks for S 2s region, comparison among state-of-the-art CBS photocathodes for PEC application.

Acknowledgement

The authors acknowledge Catalisti VLAIO (Vlaanderen Agentschap Innoveren & Ondernemen) for their funding through the Moonshot SYN-CAT project (HBC.2020.2614). DRS acknowledges funds from the Fonds voor Wetenschappelijk Onderzoek – Vlaanderen (FWO) for the fellowship (No. 11PJZ24N). B.J. and A.H. acknowledge the financial support from the FWO project VS06724N. SS acknowledges funding from the European Union's Horizon Europe program under the Marie Skłodowska-Curie Grant Agreement No. 101067667. DRS thanks Dr. Vishal Jose for the engaging and enriching discussions.

References

(1) Meng, X.; Liu, J.; Zheng, Q.; Li, S.; Xiao, H.; Huang, J.; Ma, L.; Liu, Y.; Tang, J. Gold-Crowned Bismuth-Based Nanocomposites for Sonodynamic, Photothermal, and

Chemotherapeutic Cancer Therapy. *ACS Applied Materials & Interfaces* **2023**, *15* (50), 58041-58053. DOI: 10.1021/acsami.3c08071.
(2) Chen, Q.; Ma, Y.; Qi, B.; Zhang, T.; Wang, L.; Shi, J.; Lan, X. Z-scheme Bi/AgBiS2/P25 for enhanced CO2 photoreduction to CH4 and CO with photo-themal synergy. *Applied Surface Science* **2021**, *555*, 149648. DOI: https://doi.org/10.1016/j.apsusc.2021.149648.
(3) Pai, N.; Lu, J.; Senevirathna, D. C.; Chesman, A. S. R.; Gengenbach, T.; Chatti, M.; Bach, U.; Andrews, P. C.; Spiccia, L.; Cheng, Y.-B.; Simonov, A. N. Spray deposition of AgBiS2 and Cu3BiS3 thin films for photovoltaic applications. *J. Mater. Chem. C* **2018**, *6* (10), 2483-2494, 10.1039/C7TC05711C. DOI: 10.1039/C7TC05711C.
(4) Deshmukh, S. G.; Kheraj, V. A comprehensive review on synthesis and characterizations of Cu3BiS3 thin films for solar photovoltaics. *Nanotechnol. Environ. Eng.* **2017**, *2* (1), 15. DOI: 10.1007/s41204-017-0025-8.
(5) Mesa, F.; Dussan, A.; Gordillo, G. Evidence of trapping levels and photoelectric properties of Cu3BiS3 thin films. *Physica B: Condensed Matter* **2009**, *404* (23), 5227-5230. DOI: https://doi.org/10.1016/j.physb.2009.08.302.
(6) Verónica, E.; Nair, M. T. S.; Nair, P. K. Semiconducting Cu3BiS3 thin films formed by the solid-state reaction of CuS and bismuth thin films. *Semicond. Sci. Technol.* **2003**, *18* (2), 190. DOI: 10.1088/0268-1242/18/2/322.
(7) Kocman, V.; Nuffield, E. W. The crystal structure of wittichenite, Cu3BiS3. *Acta Crystallogr., Sect. B: Struct. Crystallogr. Cryst. Chem.* **1973**, *29* (11), 2528-2535. DOI: 10.1107/s0567740873006953.
(8) Mohan, R. Green bismuth. *Nat. Chem.* **2010**, *2* (4), 336-336. DOI: 10.1038/nchem.609.
(9) Razmara, M. F.; Henderson, C. M. B.; Pattrick, R. A. D.; Bell, A. M. T.; Charnock, J. M. The crystal chemistry of the solid solution series between chalcostibite (CuSbS2) and emplectite (CuBiS2). *Mineral. Mag.* **1997**, *61* (404), 79-88. DOI: 10.1180/minmag.1997.061.404.08.
(10) Yang, Y.; Xiong, X.; Yin, H.; Zhao, M.; Han, J. Study of copper bismuth sulfide thin films for the photovoltaic application. *J. Mater. Sci.: Mater. Electron.* **2019**, *30* (2), 1832-1837. DOI: 10.1007/s10854-018-0455-5.
(11) Huang, D.; Li, L.; Wang, K.; Li, Y.; Feng, K.; Jiang, F. Wittichenite semiconductor of Cu3BiS3 films for efficient hydrogen evolution from solar driven photoelectrochemical water splitting. *Nat. Commun.* **2021**, *12* (1), 3795. DOI: 10.1038/s41467-021-24060-5.
(12) Joos, B.; Elen, K.; van den Ham, J.; Meulendijks, N.; Buskens, P.; Paulus, A.; Wouters, K.; Manca, J.; D'Haen, J.; Shukla, S.; Vermang, B.; Van Bael, M.; Hardy, A. Facile Aqueous Solution-Gel Route toward Thin Film CuBi2O4 Photocathodes for Solar Hydrogen Production. *Advanced Sustainable Systems* **2023**, *7* (8), 2300083. DOI: https://doi.org/10.1002/adsu.202300083.
(13) Chen, G.; Li, J.; Chen, S.; Huang, Z.; Wu, M.; Zhao, J.; Wang, W.; Lin, H.; Zhu, C. Low cost oxide-based deposition of Cu2FeSnS4 thin films for photovoltaic absorbers. *Materials Chemistry and Physics* **2017**, *188*, 95-99. DOI: https://doi.org/10.1016/j.matchemphys.2016.12.024.
(14) Woods-Robinson, R.; Han, Y.; Zhang, H.; Ablekim, T.; Khan, I.; Persson, K. A.; Zakutayev, A. Wide Band Gap Chalcogenide Semiconductors. *Chemical Reviews* **2020**, *120* (9), 4007-4055. DOI: 10.1021/acs.chemrev.9b00600.
(15) Cui, W.; Zhang, Y.; Chen, J.; Zhao, C.; Li, Y.; Chen, Y.; Lee, M.-H. Comparative Study on Surface Structure, Electronic Properties of Sulfide and Oxide Minerals: A First-Principles Perspective. In *Minerals*, 2019; Vol. 9.

(16) Nuffield, E. W. Studies of mineral sulpho-salts; XI, Wittichenite (klaprothite). *Econ. Geol.* **1947**, *42* (2), 147-160. DOI: 10.2113/gsecongeo.42.2.147.
(17) Zhang, L.; Jin, X.; Yuan, C.; Jiang, G.; Liu, W.; Zhu, C. The effect of the sulfur concentration on the phase transformation from the mixed CuO-Bi2O3 system to Cu3BiS3 during the sulfurization process. *Appl. Surf. Sci.* **2016**, *389*, 858-864. DOI: https://doi.org/10.1016/j.apsusc.2016.08.003.
(18) Hlaing Oo, W. M.; Johnson, J. L.; Bhatia, A.; Lund, E. A.; Nowell, M. M.; Scarpulla, M. A. Grain Size and Texture of Cu2ZnSnS4 Thin Films Synthesized by Cosputtering Binary Sulfides and Annealing: Effects of Processing Conditions and Sodium. *Journal of Electronic Materials* **2011**, *40* (11), 2214-2221. DOI: 10.1007/s11664-011-1729-3.
(19) Chae, S. Y.; Yoon, N.; Jun, M.; Hur, S. H.; Lee, M.; Kim, B.; Kim, J. Y.; Park, E. D.; Park, J. H.; Joo, O. S. Investigation of Grain Growth in Chalcopyrite CuInS2 Photoelectrodes Synthesized under Wet Chemical Conditions for Bias-Free Photoelectrochemical Water Splitting. *Solar RRL* **2024**, *8* (20), 2400518. DOI: https://doi.org/10.1002/solr.202400518.
(20) Rath, T.; Marin-Beloqui, J. M.; Bai, X.; Knall, A.-C.; Sigl, M.; Warchomicka, F. G.; Griesser, T.; Amenitsch, H.; Haque, S. A. Solution-Processable Cu3BiS3 Thin Films: Growth Process Insights and Increased Charge Generation Properties by Interface Modification. *ACS Applied Materials & Interfaces* **2023**, *15* (35), 41624-41633. DOI: 10.1021/acsami.3c10297.
(21) Whittles, T. J.; Veal, T. D.; Savory, C. N.; Yates, P. J.; Murgatroyd, P. A. E.; Gibbon, J. T.; Birkett, M.; Potter, R. J.; Major, J. D.; Durose, K.; Scanlon, D. O.; Dhanak, V. R. Band Alignments, Band Gap, Core Levels, and Valence Band States in Cu3BiS3 for Photovoltaics. *ACS Appl. Mater. Interfaces* **2019**, *11* (30), 27033-27047. DOI: 10.1021/acsami.9b04268.
(22) Moldovan, D.; Yamakov, V.; Wolf, D.; Phillpot, S. R. Scaling Behavior of Grain-Rotation-Induced Grain Growth. *Physical Review Letters* **2002**, *89* (20), 206101. DOI: 10.1103/PhysRevLett.89.206101.
(23) Wasim, S. M.; Marín, G.; Marquez, R.; Rincón, C. On the effect of structural disorders on the Urbach's tails of ternary chalcopyrite semiconductors and related ordered defect compounds. *Journal of Applied Physics* **2020**, *127* (3). DOI: 10.1063/1.5131636.
(24) Caselli, V. M.; Wei, Z.; Ackermans, M. M.; Hutter, E. M.; Ehrler, B.; Savenije, T. J. Charge Carrier Dynamics upon Sub-bandgap Excitation in Methylammonium Lead Iodide Thin Films: Effects of Urbach Tail, Deep Defects, and Two-Photon Absorption. *ACS Energy Letters* **2020**, *5* (12), 3821-3827. DOI: 10.1021/acsenergylett.0c02067.
(25) Walter, M. G.; Warren, E. L.; McKone, J. R.; Boettcher, S. W.; Mi, Q.; Santori, E. A.; Lewis, N. S. Solar Water Splitting Cells. *Chemical Reviews* **2010**, *110* (11), 6446-6473. DOI: 10.1021/cr1002326.
(26) Mamun, A. A.; Billah, A.; Anisuzzaman Talukder, M. Effects of activation overpotential in photoelectrochemical cells considering electrical and optical configurations. *Heliyon* **2023**, *9* (6), e17191. DOI: https://doi.org/10.1016/j.heliyon.2023.e17191.
(27) de la Fuente, B.; Khurana, D. A.; Vereecken, P. M.; Hubin, A.; Hauffman, T. Nano-TiO2/TiN Systems for Electrocatalysis: Mapping the Changes in Energy Band Diagram across the Semiconductor|Current Collector Interface and the Study of Effects of TiO2 Electrochemical Reduction Using UV Photoelectron Spectroscopy. *ACS Applied Materials & Interfaces* **2024**, *16* (37), 49926-49934. DOI: 10.1021/acsami.4c09736.
(28) Liu, G.; Zheng, F.; Li, J.; Zeng, G.; Ye, Y.; Larson, D. M.; Yano, J.; Crumlin, E. J.; Ager, J. W.; Wang, L.-w.; Toma, F. M. Investigation and mitigation of degradation mechanisms in Cu2O

photoelectrodes for CO2 reduction to ethylene. *Nature Energy* **2021**, *6* (12), 1124-1132. DOI: 10.1038/s41560-021-00927-1.
(29) Pletcher, D.; Greff, R.; Peat, R.; Peter, L. M.; Robinson, J. 2 - Steady state and potential step techniques. In *Instrumental Methods in Electrochemistry*, Pletcher, D., Greff, R., Peat, R., Peter, L. M., Robinson, J. Eds.; Woodhead Publishing, 2010; pp 42-75.
(30) Mesa, F.; Chamorro, W.; Hurtado, M. Optical and structural study of In2S3 thin films growth by co-evaporation and chemical bath deposition (CBD) on Cu3BiS3. *Applied Surface Science* **2015**, *350*, 38-42. DOI: https://doi.org/10.1016/j.apsusc.2015.04.032.
(31) Yang, J.; Wang, D.; Han, H.; Li, C. Roles of Cocatalysts in Photocatalysis and Photoelectrocatalysis. *Accounts of Chemical Research* **2013**, *46* (8), 1900-1909. DOI: 10.1021/ar300227e.